Journal of Civil Structural Health Monitoring
https://doi.org/10.1007/s13349-025-00916-y

ORIGINAL PAPER

Experimental assessment of the performance of terrestrial laser scanners in monitoring the geometric deformations in retaining walls

Ali Algadhi[1,2,3] · Panos Psimoulis[2,3] · Athina Grizi[4] · Luis Neves[3]

Received: 15 September 2023 / Accepted: 25 January 2025

Abstract
The Terrestrial Laser Scanner (TLS) has a great potential to be used in monitoring structures, specifically retaining walls, due to its fast acquisition and contactless function. However, previous research showed that the accuracy of deformation estimation using the TLS varied between few millimeters to a few centimeters. The Structural Health Monitoring (SHM) of retaining walls is executed according to their serviceability limits, and has to be taken with a tolerance of a few millimeters. Therefore, the aim in this study is to propose methods and approaches that ensure that the accuracy of the deformation estimation using the TLS is within $1-2$ mm. This study is based on experimental assessment, where the main scenarios of geometric deformations in retaining walls are simulated through an experimental device (i.e., wooden sheet). The wooden sheet was scanned by a TLS from distance varying from $10-27$ m with scanning angle varying between 0° and 20°. The wooden sheet was designed to simulate three main scenarios of deformation (i.e., lateral displacement, settlement and tilt) with amplitudes varying from 2 to 16 mm and 0.2° to 1.6° for tilt. This study presents a holistic attempt based on controlled experiments to evaluate the performance in monitoring deformation, using a multi-parametric analysis and identifying approaches to enhance the application of TLS in monitoring deformation of wall-type structures, such as retaining wall. The TLS measurements were compared to robotic total station measurements as well as absolute measurements using a ruler. These strategies should enhance the efficient use of the TLS in monitoring small geometric deformations.

Keywords TLS · SHM · Geometric deformations · C2C · C2M · M3C2 · Retaining wall · LiDAR

1 Introduction

Retaining walls are typically monitored according to the serviceability limits, which are expressed mainly by geometric deformations [3, 6]. The use of remote-sensing techniques for deformation monitoring of structures is considered a cost and time-efficient method with limited health and safety risks related to the remote-sensing measurements procedure [11, 24]. Photogrammetry and laser scanning are the two broadly applied contactless techniques for generating 3D point clouds [14] or even structural profiles for the dynamic response [10]. The geometric deformations can be caused by load fluctuations, such as temperature variation, and are very small (i.e., few millimeters), which is difficult to be captured by GNSS measurements as the deformation amplitude is smaller than a quarter of the satellite signal's wavelength [22, 23].

Research studies, as reported by Kim et al. [14], have shown that photogrammetry can provide an estimation of the structural deformation with an accuracy of few centimeters.

✉ Ali Algadhi
aalgadhi@ksu.edu.sa

Panos Psimoulis
Panagiotis.Psimoulis@nottingham.ac.uk

Athina Grizi
a.grizi@pde.gov.gr

Luis Neves
Luis.Neves@nottingham.ac.uk

1 Department of Civil Engineering, King Saud University, Riyadh, Saudi Arabia

2 Nottingham Geospatial Institute, University of Nottingham, Nottingham, UK

3 Department of Civil Engineering, University of Nottingham, Nottingham, UK

4 Region of Western Greece, Patras, Greece

Published online: 22 February 2025

However, the photogrammetry solution is affected by the properties of the camera (e.g., the focal length), the distance between the camera and the object [15, 20], and the environmental and lighting conditions, such as shadowed facades [5]. To monitor the geometric deformations of retaining walls during and after construction, the level of accuracy of photogrammetry measurements is not always adequate, especially with large scanning distances [14, 20]. Therefore, Kim et al. [14] reported that LiDAR sensors, involving Terrestrial and Mobile Laser Scanners (TLS and MLS), are commonly used for monitoring the geometric deformations.

The TLS was tested in monitoring retaining walls by Oskouie et al. [21] who proposed a methodology for monitoring a Mechanically Stabilized Earth (MSE) wall using TLS, where they scanned the wall once and introduced the deformation to the wall manually. To validate their results, they simulated different deformation scenarios involving four types of deformations (lateral displacement, settlement, absolute tilt, and relative tilt). Their results showed that the TLS had an error of $1-2.5$ mm depending on the scanning range, angle of incidence, and angular resolution. Seo et al. [28] investigated the performance of TLS in monitoring a soil mixing wall with a ring beam on top, which are subjected to construction work. They checked the accuracy of the TLS for estimating the daily and cumulative deformation for the wall compared to measurements by inclinometer and total station. They concluded that the TLS could estimate the cumulative lateral displacement (maximum of 25 mm for the ring beam, and 50 mm for the wall), but not the incremental lateral displacement (maximum of 3 mm for the ring beam, and 4 mm for the wall) of the wall.

Seo [26] tested the accuracy of the TLS measurements in estimating the tilt of retaining structures via a calibration test where a zig zag-shaped wooden panel was used to simulate the surface of the retaining wall. The results showed an accuracy of 0.15° in detecting the tilt of the panel. Li et al. [18] also tested the accuracy of the TLS in monitoring the change in the length of the walls of a structure using two scans from the same day (i.e., with no deformation) as a calibration test, and they had an accuracy of within ± 6 mm. Lienhart [19] discussed some potential errors in deformation estimation using the TLS, such as surface material, weather condition and the inclination angle to the monitored surface.

For monitoring retaining structures using the MLS, Aldosari et al. [3] and Al-Rawabdeh et al. [2] proposed a methodology of processing and estimating the deformations of textured and smooth MSE wall panels, respectively, under global serviceability measures (i.e., longitudinal and transversal angular distortions) and local performance measures (i.e., finding the translations and rotations that fits the local coordinate system for each panel with the wall coordinate system). Furthermore, the normal distances between the corners of each panel and the fitted plane of the neighboring panels were used as an additional local serviceability measure. The results by Aldosari et al. [3] showed that the difference in the estimation of the angular distortion of the walls between the MLS and TLS measurements was around $0.001-0.003$, whereas Al-Rawabdeh et al. [2] reported an agreement of around 5 mm between MLS/TLS and an onsite profiler gage in estimating the normal distances between the panels. Kalenjuk et al. [13] focused on the automation of the deformation analysis methodology using MLS point clouds for retaining walls with a case study of anchored walls with concrete panels, in comparison to measurements by optical surveys with 209 targets for four retaining walls. The tilt was measured with an accuracy of 0.03°, with a confidence level of 95%.

Three methods for the distance calculation between two point clouds have been broadly used in research related to deformation monitoring: Cloud-to-Cloud (C2C), Cloud-to-Mesh (C2M), and Multiscale-Model-to-Model-Cloud-Comparison (M3C2) methods [27]. These methods calculate the distance between points/group of points in the two point clouds [16]. Additionally, the Piecewise Alignment Method (PAM) was also used by Seo et al. [28], which transforms a selected piece in the reference cloud to match the same piece in the deformed cloud using the Iterative Closest Point (ICP) technique. The ICP method, developed by Besl and McKay [7], iterates using the least squares method to find the best transformation parameters that will perform the fine registration of one point cloud to best-fit another, with the assumption that these two point clouds are taken for the same object. Therefore, this method is more applicable for applications such as cloud registration rather than deformation analysis.

The performance of the C2C, C2M and M3C2 was tested for monitoring geometric deformations by Zhao et al. [29] through artificially moving one point cloud and obtaining the deformation using the three methods. They obtained different estimations of the deformation depending on the monitored surface (i.e., ring beam and soil mixing wall) and the method used for the deformation estimation (i.e., C2C, C2M and M3C2). Lague et al. [16] and Seo et al. [27] also tested the C2C, C2M and M3C2 methods on estimating the deformation of generated point clouds with normal noise distribution which are shifted by a specific value, and they obtained various estimations by each method. This shows potential variance in deformation estimation caused by the method of distance calculation; however, the accuracy of these methods in estimating the geometric deformation should be validated using two independent point clouds (i.e., not manually shifted point clouds).

Although the presented studies showed that the LiDAR sensors had an accuracy in the millimeter level, some research studies that were reported in Kim et al. [14] showed accuracy in the *cm* level; and therefore they propose that the performance of the TLS requires further validation with other more accurate techniques before being used for monitoring geometric deformations. Kaartinen et al. [12] suggested further investigation of the performance of the TLS by conducting experiments where the TLS is tested with various scanning distance and angle of incidence. The type and the amplitude of deformation were also examined by Oats et al. [20] and Seo et al. [27]. The method of distance calculation between the point clouds is also another factor that influences the accuracy of the deformation estimation [12, 27]. Therefore, the scope of this study is to assess the performance of TLS in monitoring three common types of geometric deformations in retaining walls, or similar surface wall-type civil engineering structures, based on controlled environment and compared to measurements from more accurate devices, such as absolute measurements and measurements with a robotic total station.

The experimental device (i.e., the wooden sheet) is used to simulate three types of deformation in retaining walls: (i) lateral displacement, (ii) settlement, and (iii) tilt about the transverse axis of the wall. The amplitude of deformation was varying between 2 and 16 mm for the lateral displacement/settlement and $0.2° - 1.6°$ for the tilt. Various methods of the deformation analysis of the point clouds were applied, and the performance of the TLS was compared to robotic total station measurements as well as absolute measurements using a ruler. Four objectives are designed in this research; (i) deformation analysis using two single scans in the condition that both scans (i.e., at the initial and deformed states) were taken at same location, (ii) deformation analysis using two single scans in the condition that the latter scan (i.e., at the deformed state) was taken from different scanning position than the scan initial undeformed state, (iii) deformation analysis using multiple scans (total of six scans) for the same surface, and (iv) investigation for classification of the type of deformation (i.e., lateral displacement, settlement or tilt) based on the point clouds. These should develop an understanding of the deformation analysis for the point clouds as well as ensure the level of accuracy to be within $1 - 2$ mm.

A preliminary analysis of part of this experimental was presented in Algadhi et al. [4], including only the results of the lateral displacement scenario. The current study does not only involve additional deformation scenarios (i.e., settlement and tilt) to compare them with the lateral displacement, but also involve additional analysis, such as the (i) analysis based on different scanning positions, (ii) analysis using multiple scans for the same epoch, and (iii) the analysis of point clouds to identify the type and amplitude of deformation.

2 Experimental equipment

The experimental device (Fig. 1) was designed considering three of the main types of global deformations in retaining walls: (i) lateral displacement, (ii) vertical displacement/settlement, and (iii) tilt about the transverse axis of the retaining wall, without reflecting on the potential complicated mechanism which produces the deformation, which was not in the scope of this study. The frame consisted of two parts: (i) a wooden sheet (1 m × 1.5 m), as shown in Fig. 1a, simulating the visible front surface of the retaining wall, which was the monitored surface, and (ii) a lifting frame (Fig. 1b), which was used to introduce the desirable deformation. Five paper black/white targets were glued on five key locations of the wooden sheet, i.e., the four corners and the center of the wooden sheet, to provide a representation of the wooden sheet (Fig. 1a).

The frame was supported on four bolts (Fig. 1b), which were also used to introduce the deformation of (i) settlement by adjusting evenly the height of the four bolts and (ii) tilt by adjusting the two rear bolts and according to the distance between the two front and rear bolts, to create the desirable angle of tilt on the lifting frame and consequently to the wooden sheet. The lateral displacement, however, was introduced via an additional bolt which was installed at the support of the wooden sheet, which could be adjusted to the desirable lateral displacement, thanks to the attached metallic measuring tape (Fig. 1c).

3 Experimental methods

Three types of global geometric deformations were simulated in this experiment with various amplitudes: (i) lateral displacement, (ii) settlement, and (iii) tilt about the transverse axis of the wooden sheet. The mechanism of introducing the deformations was presented in Sect. 2. Each deformation scenario was simulated in a separate day to spread the workload, and thus the processing was done to each day independently.

Both lateral displacement and subsidence were ranging between 2 mm and 16 mm, whereas the tilt was in the range between 0.2° and 1.6°. The TLS, namely the Leica RTC360, was set to scan from six scanning positions; scanning range varying between 10 m and 27 m and scanning angle of 0° and 20° (i.e., angle of incidence of 90° and 70°), whereas the RTS, namely the Leica TS30, was set at one location with a distance of about 20 m and angle of about 0° to the wooden sheet (i.e., angle of incidence of 90°). Table 1 summarizes the deformation scenarios and the scanning setups for the conducted experiments.

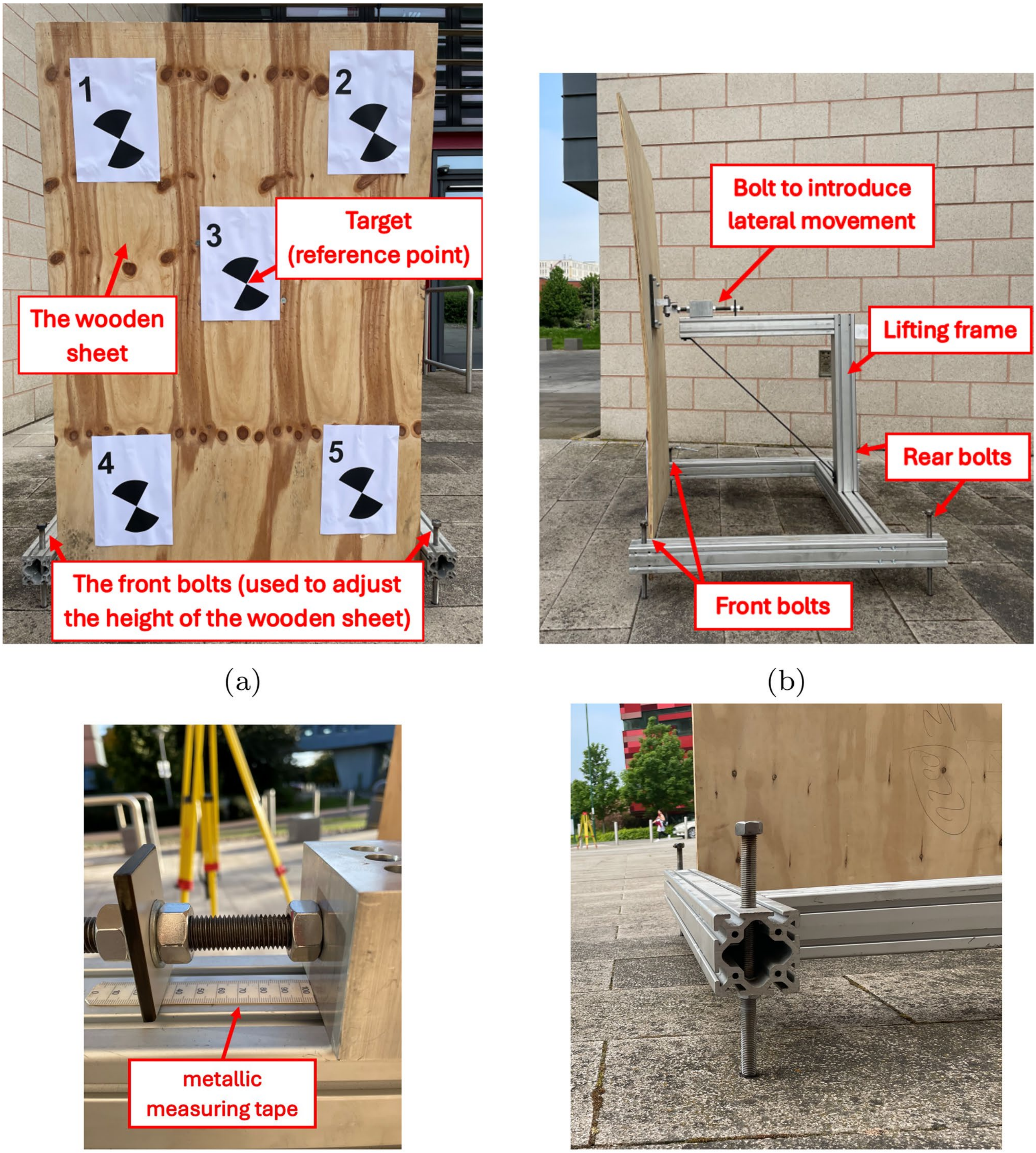

(a) (b) (c) (d)

Fig. 1 Design of the experimental equipment: **a** front view showing the wooden sheet, **b** side view showing the lifting frame, **c** bolt that was used to introduce lateral displacement and the attached metallic measuring tape, and **d** supporting bolt for the wooden sheet to introduce settlement and tilt

Table 1 Experiment setup of the three examined global geometric deformations

Scan setup (for the TLS)		Scenarios of geometric deformations		
Range (*m*)	Scanning angle (°)	Lateral displacement (*mm*)	Settlement (*mm*)	Tilt (°)
10	0 (orthogonal)	Initial	Initial	Initial
20	20	2	2	0.2
27		4	4	0.4
		8	8	0.8
		16	16	1.6

Total number of scans for the TLS = 3 (ranges) × 2 (scanning angles) × 5 (amplitudes of deformation) = 30 scans per deformation scenario

Three static targets (Leica GZT21) were used to register the measurements from the RTS and TLS scans to a local coordinate system. The experiment was conducted outdoor, and all the scans associated with one deformation scenario were completed within one day. For example, the scans of the lateral displacement scenario, including five deformation amplitudes and six scanning positions (total of 30 scans), were captured on the same day. The same methodology was repeated for the settlement and tilt experiments. Figure 2 shows the experiment setup and the location of the wooden sheet, the static targets, the RTS, and the six scanning positions of the TLS.

The first step for each experiment was to survey the static targets using the RTS to introduce the local coordinate system and to ensure that both the RTS and the static targets remained stationary during the experiment. After that, the wooden sheet was scanned by the TLS from the six locations with no introduced deformation (initial-undeformed state). Meanwhile, the RTS was used to survey the glued targets on the wooden sheet. These coordinates of the glued targets were considered the initial undeformed coordinates of the paper targets. In the next stage, a deformation was introduced to the wooden sheet, according to the details presented in Table 1. RTS and TLS were then used to measure and scan, respectively, the wooden sheet in the deformed state. Prior to any scanning, the Leica GZT21 targets were

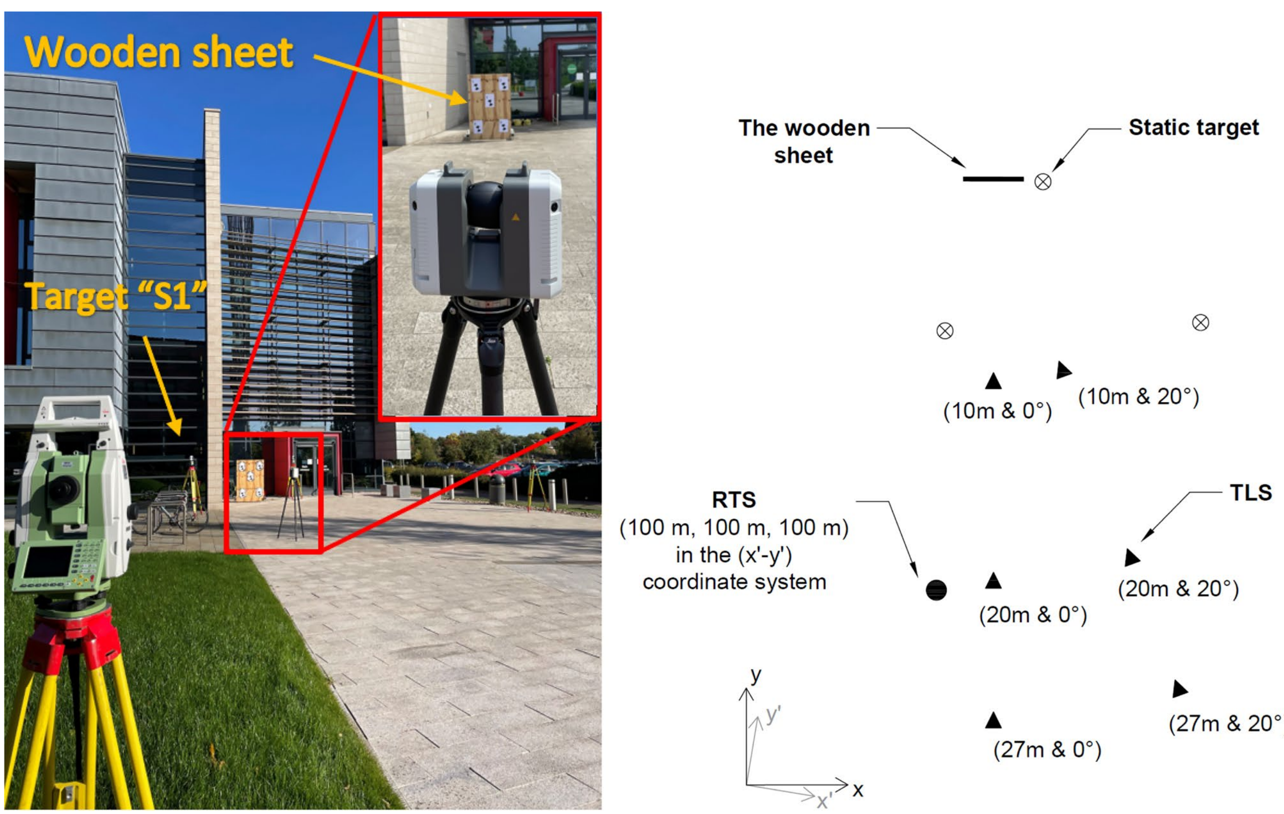

(a) (b)

Fig. 2 Experiment setup: **a** Overview of the experimental setup, with RTS located at the front and indicating at the background the TLS, the wooden sheet, and one of the static targets for registration. **b** Plan view of the experiment site; where there are indicated (i) the scanning positions (triangles) of the TLS with different scanning distances and angles, (ii) the static targets *S*1, *S*2, and *S*3 and (iii) the 2D Cartesian coordinate system as it was initially defined ($x' - y'$ plane) and then transformed to $x - y$ plane oriented toward the TLS laser-scanner at each scanning position to minimize the error on defining the coordinates of the Leica GZT21 targets caused by the angle of incidence. This procedure was done for all the deformation scenarios (i.e., lateral displacement, settlement and tilt) and amplitudes of deformation.

The TLS was set to scan with the highest available resolution (i.e., 3 mm at 10 m) to have the best representation of the scanned surface at each scanning position, and the "double scan" function was used to remove any dynamic objects [17]. On the other hand, the RTS was configured in reflectorless measuring mode to survey the targets that were glued to the wooden sheet (Fig. 1a), and the Leica GZT21 targets (Fig. 2b) using the arithmetic mean of face left and face right to mitigate instrumental errors, such as collimation error.

4 Design of the local coordinate system and cloud registration

The point clouds were taken from many different scanning positions, and therefore these clouds must be registered in the same coordinate system to perform the desired analysis. Not only that but also additional measurements were taken using RTS, and hence they must be registered in the same coordinate system to allow for the comparison between the measurements. The general concept was to align the y−axis to the direction where the lateral displacement was calculated for the wooden sheet, whereas the z− axis to be aligned to the longitudinal axis of the wooden sheet (i.e., the sheet's height).

The local coordinate system was defined using the RTS measurements. The initial (i.e., as defined in the field) coordinate system $x'y'z'$ was defined based on the location of the RTS, as reference point of known local coordinates ($x'_o = 100\,\mathrm{m}$, $y'_o = 100\,\mathrm{m}$ and $z'_o = 100\,\mathrm{m}$), and defining the y'−axis as the axis pointing toward the target S_1. This coordinate system was shown in Fig. 2b as the preliminary coordinate system ($x' - y'$). In that coordinate system, the orientation of the wooden sheet in the $x' - y'$ plane was defined based on the RTS measurements of the five paper targets on the wooden sheet and fitting a line by using the linear regression method (Fig. 3). Then, the relative angle between the wooden sheet and the x'−axis was used to rotate the coordinate system about the z'−axis. The final xyz coordinate system had the x−axis and y−axis parallel and perpendicular to the plane of the wooden sheet, respectively. Hence, the lateral displacement was expressed along the y−axis, the settlement along the z−axis and the tilt based on the relative rotation about the x−axis. The five targets were not perfectly aligned in $x - y$ plane, mainly due to small tilt of the wooden sheet about x−axis and slightly bended surface of the wooden sheet (Fig. 1).

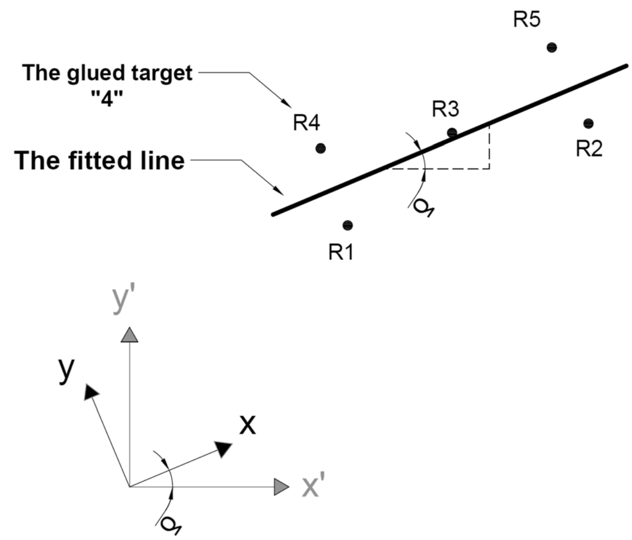

Fig. 3 Top view of the wooden sheet showing the preliminary and final coordinate systems

Each TLS scan was then registered to this final coordinate system ($x - y$) using the three static targets ($S_1 - S_3$), as shown in Fig. 2b. The registration was done using the Helmert method of coordinate transformation [25], which requires seven parameters to be computed; (i) three translations ($\Delta X, \Delta Y, \Delta Z$), (ii) three rotations around x, y and z−axes (r_x, r_y, r_z), and (iii) one scale factor (μ). The 3D (x, y, z) known coordinates of the three static targets defined nine observations, which were used to form an over-determined equation system of nine equations and seven unknowns, which was solved with the least squares adjustment method. This process was performed for each of the three experimental scenarios of deformation separately as each deformation scenario (i.e., lateral displacement, settlement and tilt) was simulated on a separate day.

5 Methods of deformation estimation

Five methods were performed for estimating the geometric deformations: (i) target method, (ii) cloud-mean method, (iii) C2C method, (iv) C2M method, and (v) M3C2 method. The first uses the point-based analysis to monitor the deformations of the wooden sheet at specific points (Fig. 1a). The cloud-mean method utilized involved estimating the displacement along desirable direction by monitoring the change in the position of the arithmetic mean of the reference and deformed clouds along that direction. Both the target and cloud-mean methods were used for estimating the lateral displacement and settlement via the following equations:

$$LD_i = \bar{y}_i - \bar{y}_0 \tag{1}$$

$$S_i = \bar{z}_i - \bar{z}_0 \tag{2}$$

where LD_i and S_i represent the lateral displacement and the settlement for the wooden sheet at the epoch i (i.e., the other amplitudes of deformation), respectively. $\bar{y}_0$ and $\bar{z}_0$ represent the coordinates/arithmetic mean of cloud along the $y-$ and $z-$axes at the initial undeformed state, and $\bar{y}_i$ and $\bar{z}_i$ are the coordinates/arithmetic mean of cloud along the $y-$ and $z-$ axes at the epoch i.

The C2C method utilized was based on the calculation of the distance between each point of the deformed state cloud and its nearest point in the reference state cloud. This was improved by applying a local height function, where for each point of the reference cloud, six neighboring points were determined to create a local surface in the point cloud against which the point of the deformed state were compared. Hence, the C2C distance was calculated via the minimum distance between the point in the deformed cloud and the local surface of the reference cloud. Similarly, the C2M method utilized was performed between each point in the deformed cloud and a mesh, that was created for the reference point cloud using a fit plane with "2.5D quadric" equation. The distance was calculated as the minimum Euclidean distance between the points in the deformed cloud and the mesh of the reference cloud.

The M3C2 method was executed in two stages. For each point in the reference cloud, the first step was defining a local surface with a specific diameter D (0.018 m in this experiment), which was used to define the normal direction for that local surface. The normal direction was used as the local axis that the distance between the two clouds were calculated. The second step was defining a projection scale d (0.018 m in this experiment), which was the diameter of the projected cylinder. This was used to define the local surfaces in both the reference and deformed states. The difference between the two local surfaces was recorded. To accelerate the processing time, a threshold was set to the maximum distance L that can be calculated (0.090 m in this experiment). The values presented were proposed by CloudCompare [9] based on the roughness of the point clouds, which were varying from 0.005 m to 0.014 m based on the scanning position.

The tilt of the wooden sheet about its transverse axis has been estimated through two methods: (i) target-based method, and (ii) cloud-based method. The tilt was calculated for both methods via the following equation:

$$\phi = tan^{-1}\left(\frac{m_0 - m_i}{1 + m_0 * m_i}\right) \tag{3}$$

where m_0 was the slope of the fitted line of the wooden sheet at the initial undeformed state, and m_i represents the slope of the fitted line for the wooden sheet surface at the epoch i, which in this case the other amplitudes of tilt. The tilt ϕ was the angle between the two fitted lines (i.e., the initial undeformed state and the deformed state).

The lateral displacement and the tilt were outwards (i.e., toward the TLS), whereas the settlement was downwards. All the deformations were reported as the absolute error as the direction of the error was not of interest in this research. No subsampling was performed for the point clouds to achieve the best accuracy available. The arithmetic mean of the calculated distances for the C2C, C2M and M3C2 methods was taken as the overall lateral displacement of the wooden sheet.

6 Results and discussion

Four investigations were studied: (i) analysis using scans with same scanning position, (ii) analysis using scans with different scanning position, (iii) analysis using multiple scans, and (iv) the identification of the type of deformation. Based on the results of this study, a list of strategies for the use of TLS for monitoring retaining walls is presented in the conclusion section.

6.1 Analysis using scans with same scanning position

The accuracy of the deformation estimation was examined under various (i) types of deformation, (ii) amplitudes of deformation, (iii) scanning distances, (iv) scanning angles, and (v) methods for the point cloud data analysis. The presented analysis in this section is based on comparing two single scans; the reference and deformed states of the wooden sheet, in the condition that both scans were taken from the same scanning position. For example, while using the scan of the wooden sheet at the initial state from the scanning position of (10 m & 0°) as the reference cloud, the point cloud of the deformed state was taken from the same scanning position (10 m & 0°).

The results show a high accuracy of the TLS in measuring the geometric deformations in retaining walls for the tested deformation scenarios, to the millimeter and even sub-millimeter level comparing to the absolute measurements (Fig. 4). For the measurements related to lateral displacement, all five methods of deformation estimation had similar performance unlike the settlement data, where the target and mean methods of the TLS measurements exhibited a weaker

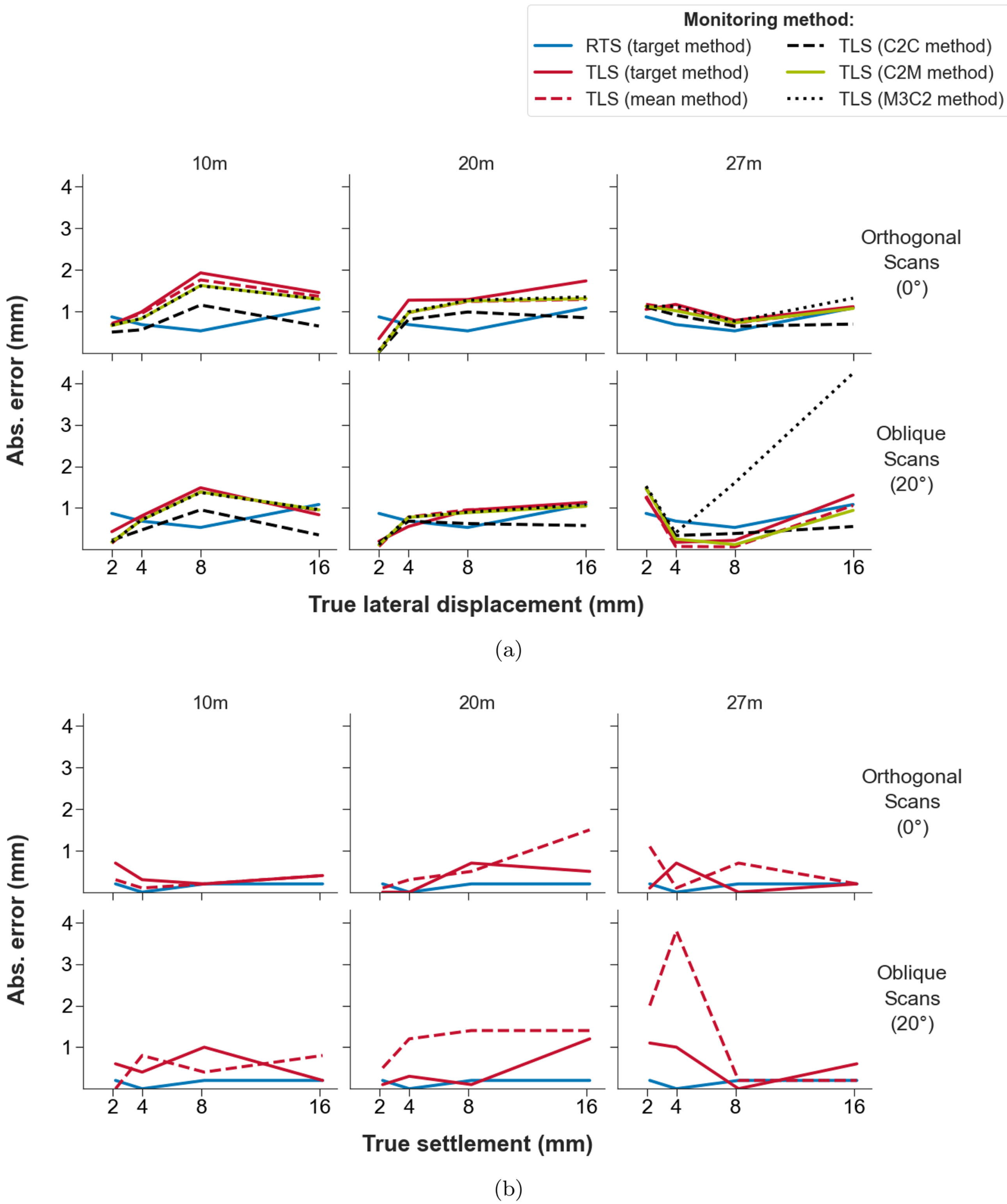

Fig. 4 Error of the RTS and TLS in defining the deformations in the wooden sheet: **a** lateral displacement, and **b** settlement

correlation. The accuracy in this experiment (i.e., $1-2$ mm) was better than the case of Acikgoz et al. [1], who had an accuracy of 3 mm using the M3C2 method, compared to the data obtained by a Total Station, and the case of Al-Rawabdeh et al. [2], who achieved an accuracy of 5 mm, with respect to an on-site profiler gage approach. The error was larger in their cases because of the additional error caused by the uncertainty in the location of the static points that were used for the registration of the point clouds. Furthermore, the analysis in this research was based on point clouds that were taken from the same scanning position, which can mitigate the errors from the scanning distance and angle.

For the estimation of the lateral displacement, Fig. 4 shows that the methods of distance calculation between the point clouds (i.e., C2C, C2M, and M3C2) had similar performance (i.e., average of 0.65 mm, 0.86 mm and 1.09 mm) as the target and cloud-mean methods (i.e., average of 0.96 mm and 0.87 mm), whereas the RTS had an average of 0.79 mm. The C2M method was the closest to the performance of the target and cloud-mean methods since the main principle of C2M is similar to the cloud-mean method by using a mesh to represent the reference point cloud (i.e., initial state), while the C2C and M3C2 methods used local surfaces. The C2C and M3C2 methods may involve additional errors if the wooden sheet was slightly moved horizontally (i.e., along the x–axis) or if inappropriate input parameters are used (e.g., inappropriate normal scale), such as the case of M3C2 method at scanning position of (27 m & 20°). Acikgoz et al. [1] also emphasized this error and said that it affects mainly the curved surfaces.

The C2C method, in this research, was the most accurate method for deformation estimation (i.e., average error of 0.65 mm), whereas Lague et al. [16] concluded that the C2C method had larger error than the C2M and M3C2 methods because it is influenced by the noise of the point clouds. The better performance in this experiment was because of comparing scans that were taken from the same location (i.e., reference and deformed clouds), resulting in having the same roughness and characteristics. Furthermore, the use of the height function improved the performance of the C2C method in this research as well as the case of Lague et al. [16]. In addition, the C2C distance was calculated purely along the y–axis, whereas the C2M distance was calculated as the minimum Euclidean distance between the points in the deformed cloud and the mesh of the reference cloud, and the direction of distance calculation for the M3C2 method was adjusted using the local surface at the point where the deformation was calculated.

The M3C2 method, unexpectedly, had a performance similar to the C2C and C2M methods, and sometimes had larger error such as the case of scanning position of (27 m & 20°). This was because the normal scale and the projection scale were fixed for all the scanning positions, as detailed in Sect. 5 while the roughness of the point clouds was different for each scanning position, which plays significant role on the estimation of the M3C2 parameters [16, 27].

Regarding the settlement, Fig. 4 shows that the performance of the TLS (i.e., average error of 0.43 mm and 0.76 mm) using the target and cloud-mean methods was better than the case of lateral displacement (i.e., average error of 0.96 mm and 0.87 mm). The patterns of the target and cloud-mean methods using the TLS measurements were not consistent unlike the case of lateral displacement, which suggests that the cloud-mean method is sensitive to the fine registration and fine cleaning of the point clouds (i.e., cropping the area of interest).

Likewise, the analysis of the accuracy of the deformation estimation was done for the tilt scenario (Fig. 5). The errors in general were within 0.1° except the case of the scans that were taken orthogonally from a scanning distance of 10 m. In this case, the patterns were systematically shifted, which suggests that the estimation of the slope of the fitted line for initial undeformed state at that scanning position (10 m & 0°) was biased. The error was caused by the registration of that cloud (the initial state) since both methods had a systematic error in the tilt estimation in Fig. 5, and that affected more the target-based than the cloud-based method due to the fact that the fitted line for the target-based method is based only on the five targets making it more vulnerable to potential errors.

6.2 Analysis using scans with different scanning positions

The cloud-mean method is contactless and capable of defining the deformation in the wooden sheet with an average error of less than 1 mm for the lateral displacement and settlement, and 0.04° for the tilt (Figs. 4 and 5), and is deemed to be less impacted by the horizontal movement (i.e., along the transverse axis) of the monitored surface. Therefore, the cloud-mean method was further investigated to study the impact of changing the scanning position between the first and latter epochs. In typical monitoring projects, it is common that the TLS would not be scanning from the same position as the first epoch (i.e., the initial scan). Therefore, the same data that was used in Sect. 6.1 was analyzed with only one difference using reference and deformed scans with different scanning positions between the first and latter epochs. For example, the scan (10 m & 0°) at the initial state of the wooden sheet was compared with the deformed scan from (20 m & 20°).

Figure 6 presents box plots for the errors when the analysis was based on: (i) reference and deformed scans that were taken from the same scanning position (the same data in Sect. 6.1), which is highlighted in blue, and (ii) deformed scans that were from a different position than the reference scan, which is highlighted in red. For each scanning position (six positions) and deformation type (three types) and amplitude (four amplitudes), the scan at the initial undeformed state was compared to the scans at the deformed state from other five scanning positions. This results in 360 deformation estimations in total ($6 \times 3 \times 4 \times 5$).

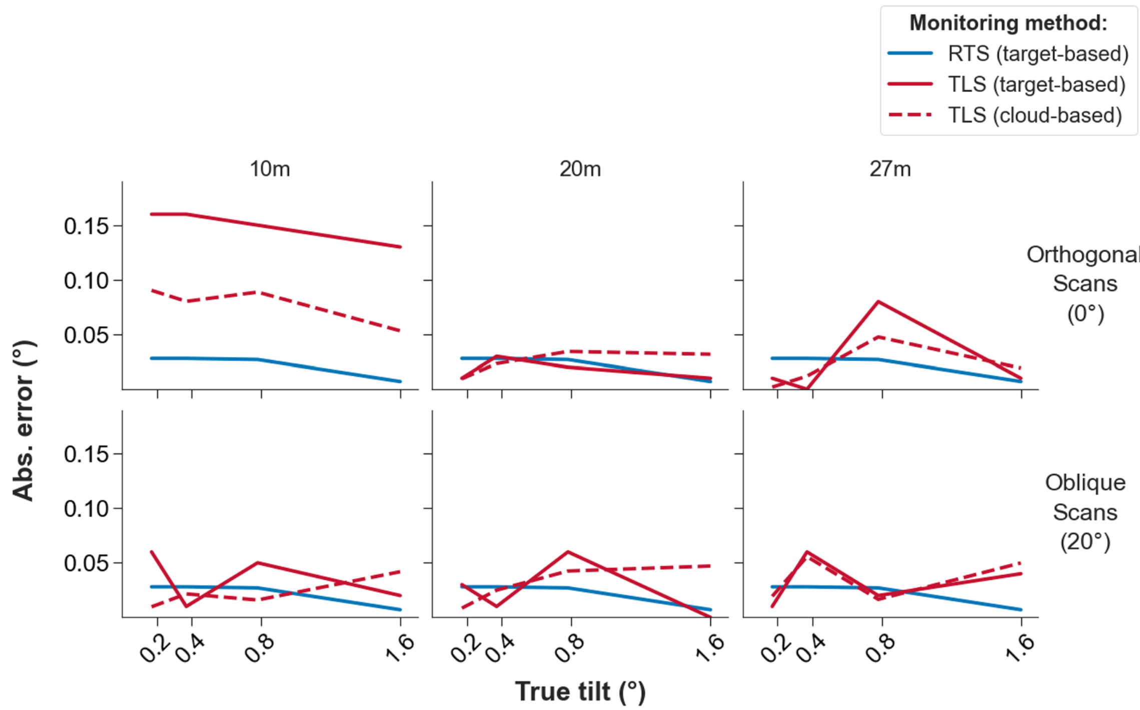

Fig. 5 Error of the RTS and TLS in defining the tilt in the wooden sheet

The change in scanning position increased the error budget for the settlement type of deformation to be 3 – 4 times the estimations that were based on analysis of point clouds from the same scanning position, unlike the other types of deformations. For the deformation of lateral displacement, the error was limited to 2 mm regardless the scanning distance, angle of incidence and deformation amplitude, and the estimation was not affected by changing scanning position. Likewise, neither the introduced angles of incidence nor the scanning distances seem to significantly affect the error in estimating the tilt in the wooden sheet if the reference and deformed scans were taken from the same location. However, it seems that the accuracy of the tilt estimation was slightly improved for longer scanning distances (i.e., > 10 m) or oblique angle of incidence (i.e., 20°)) probably because as the angle increases and the distance increases, the point cloud variation in the lateral axis becomes smaller, resulting in a more defined surface of the wooden sheet. Bolkas and Martinez [8] stated that the plane fitting residuals decreases as the scanning angle increases.

The impact of changing the scanning position on the accuracy of deformation estimation was larger for the settlement cases because it is more sensitive to the density of the point clouds than the lateral displacement or tilt. In the case of comparing two scans from different scanning positions, the density of points for the reference and deformed clouds is different. Figure 7 shows an example of histogram plots for two scans at the initial-undeformed state in the $y-$ and $z-$axes for the scans that were taken from (10 m & 0°) and (27 m & 20°). The arithmetic means of the two clouds were agreeing in the $y-$axis with 0.4 mm of difference, whereas the difference between the arithmetic means for these two point clouds along the $z-$axis was much larger (4.7 mm). In other words, although the wooden sheet was at the same deformation state (i.e., stationary), the change in scanning location from (10 m & 0°) to (27 m & 20°) caused an error in estimating the lateral displacement and settlement of 0.4 mm and 4.7 mm, respectively.

6.3 Analysis using multiple scans

Although the main approach of this chapter is to estimate the deformation by using two single scans, this section evaluates the possibility of increasing the accuracy of the deformation estimation using the TLS by combining scans that were taken from different scanning distances and angles, that enable the effect of random errors to be minimized. To test this, the scans that were taken from the six scanning stations (i.e., three scanning distances and two scanning angles) were processed in groups as one cloud.

Since all the scans were already registered in the same coordinate system, the scans were processed directly using the cloud-mean method to estimate the lateral displacement and settlement, and the cloud-based method for estimating the tilt in the wooden sheet (Fig. 8). Three types of groups were formed: (i) angle filtration, where three scans shared

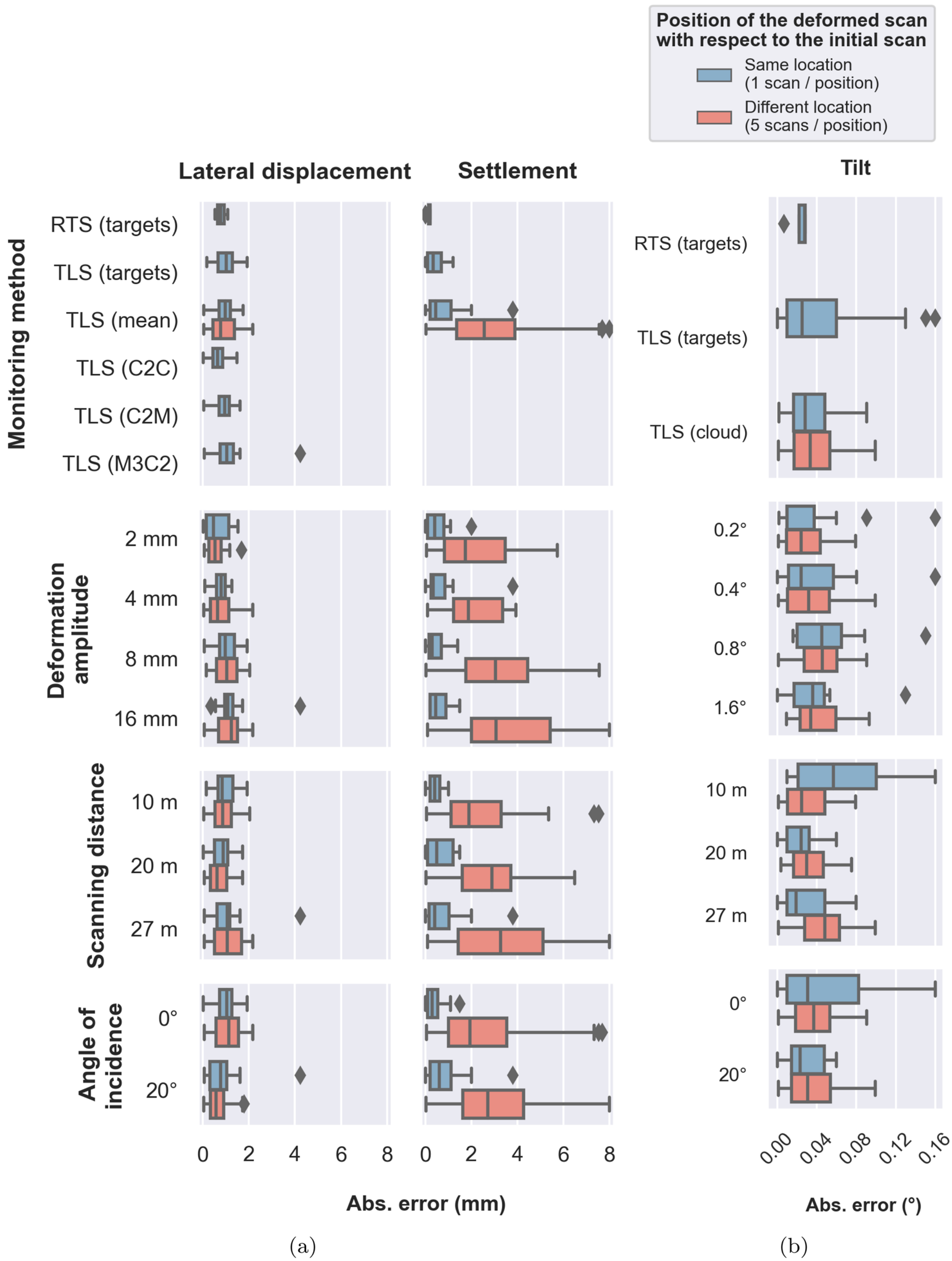

Fig. 6 Statistical summary of the deformation analysis that was based on scans that were taken from the same scanning position between the reference and deformed scans: **a** lateral displacement and settlement, and **b** tilt

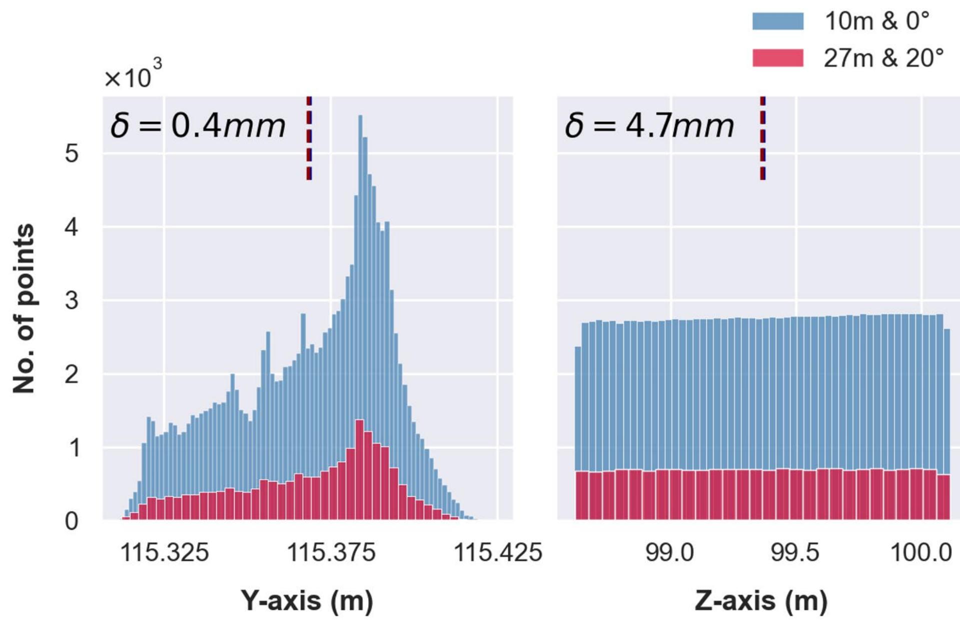

Fig. 7 Histogram plots for the point clouds that were taken at the initial state but from different scanning locations; (10 m & 0°) and (27 m & 20 °), where δ is the difference between the two arithmetic means of the two point clouds. The y–axis is the lateral axis with respect to the surface of the wooden sheet while the z–axis is the longitudinal axis along the height of the wooden sheet. The numbers in the figure represent the location of the point clouds with respect to the origin of the coordinate system as explained in Fig. 2

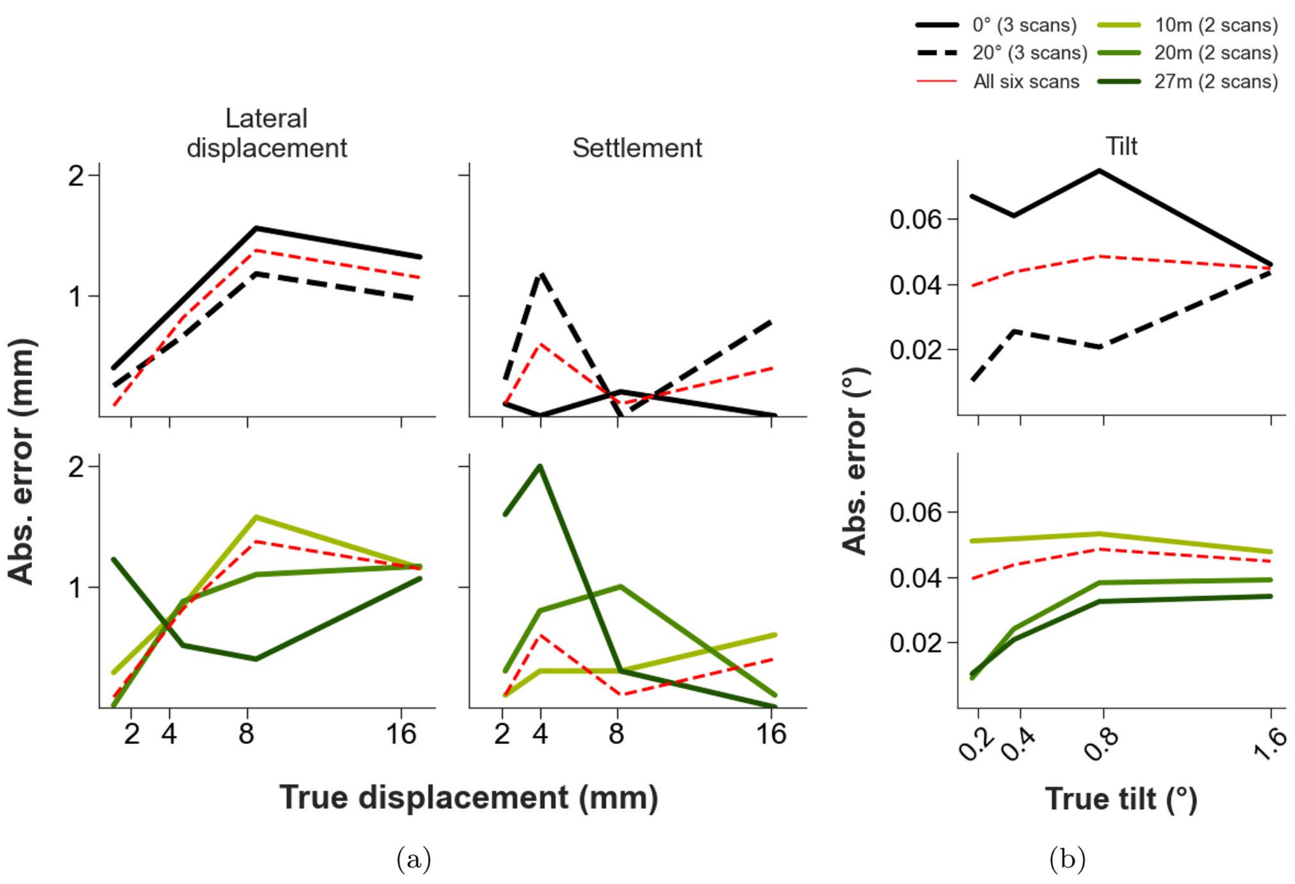

Fig. 8 Effect of using multiple scans to define the deformation in the wooden sheet: **a** lateral displacement and settlement, and **b** tilt

the same angle of incidence but different distances (e.g., 10 m & 0°, 20 m & 0° and 27 m & 0°), and is printed in green in Fig. 8, (ii) distance filtration; where two scans shared the same distance but with different angle of incidence (e.g., 10 m & 0° and 10 m & 20°), and is printed in black (solid and dashed), and (iii) the case where all the scans from the six scanning positions were used as one group, and is printed in red.

The main finding is that the performance of the TLS using all six scans (i.e., the red line) was very close to the deformation estimation using the scans with a scanning distance of 10 m (i.e., the line in light green). This is because the density of the point clouds was much larger for the scans with scanning distance of 10 m, and consequently these scans (i.e., with scanning distance of 10 m) influenced the deformation estimation. This can be seen in all the deformation scenarios; lateral displacement, settlement, and tilt.

In addition, the effect of scanning distance and scanning angle was clearer in this section, in comparison to Sect. 6.1 where the analysis was based on single scans at a specific scanning position. For the estimation of lateral displacement and tilt, the accuracy and precision of the deformation estimation was improved as the scanning distance increases, and as the angle of incidence increases. In contrast, the estimation of settlement was improved as the TLS gets closer to the scanned surface and when the scans were taken orthogonally.

6.4 Identification of the type of deformation

In the previous sections, the investigations focused on estimating the accuracy of the TLS in detecting the global geometric deformations in retaining walls for specific scenarios and types of deformation, without evaluating how a type of deformation can be defined and separated from other types. For example, on Day-1, only experiments of lateral displacement were executed and the TLS data was analyzed only for the estimation of lateral displacement. Retaining walls are subjected to various types, magnitudes and directions of loads, and therefore it is possible to have several types of deformations simultaneously. This section investigates a statistical approach to detect the type of deformation.

The Kernel Density Estimation (KDE) is a statistical method that uses kernels to build a probability density function for one random variable, and the Cumulative Distribution Function (CDF) is the probability function that shows the probability that a random variable is equal or less than a specific value. These two can be used to describe the distribution of the data, and hence were applied for the scans on each day of the experiments: Day 1 for lateral displacement; Day 2 for settlement; Day 3 for tilt. In this study, they are used to describe the distribution of the point clouds along one axis (e.g., y–axis). Figure 9 shows the KDE and CDF plots for the y– and z–axes for the three days of experiments. The lines were designed from the case where all six scans were involved.

In the y–axis, the CDF curves were (i) shifted with no change on the curve-pattern expressing the lateral displacement, with the shift depending on the displacement amplitude, or (ii) flattened and rotated with respect the top of the curve expressing the tilt deformation, where the flattening of the curve increases with the tilt deformation. The curves were almost at the same location on Day 2 for the settlement simulations as the introduced deformation was purely vertical along the z–axis. The change in the curves is clearer along the y–axis comparing to the z–axis because the spread of the points in the point clouds was smaller in the y–axis comparing to the z–axis. In other words, the range of the points was around 0.1 m and 1.5 m in the y– and z–axes, respectively. Therefore, the small change along the z–axis is hard to detect; however, the KDE could capture the small movement along the z–axis if the KDE was cropped for a smaller section, such as 0.4 m window of the 1.5 m high wooden sheet (Fig. 9). The change was only noticed on the day where the settlement was simulated. This shows the feasibility of using the point clouds to identify the dominant type of deformation in retaining structures.

7 Conclusions and future recommendations

The current study focused on the experimental assessment of the performance of the TLS in monitoring geometric deformation of civil engineering structures, such as retaining walls. We applied an approach evaluating holistically the performance of TLS and how it is affected by various parameters (scanning distance, angle, distance calculation method) and examining approaches to mitigate the TLS errors, and to detect the type and amplitude of deformation based on statistical tools (i.e., CDF and KDE analysis).

Based on the experiments and the various analysis methods that were applied, the following key points were highlighted which can result in an accuracy of $1-2$ mm in monitoring the geometric deformations of structures:

- The use of targets on the monitored surface is recommended for monitoring the settlement type deformation in the monitored structure to achieve an accuracy of $1-2$ mm. Regarding the scenarios of lateral displacement and tilt, the high level of accuracy does not require the use of targets.
- For the TLS applied in this study, the highest accuracy of deformation estimation was achieved at the scanning range of 20 m, with a scanning resolution of 3 mm at 10 m for all types of deformation.
- It was observed that using the same scanning position for the different epochs (i.e., prior and after the introduced deformation) mitigates the errors from the scanning range and angle of incidence, especially for the settlement type of deformation.
- The application of multiple scans of the surface at the same epoch does not improve the performance of the

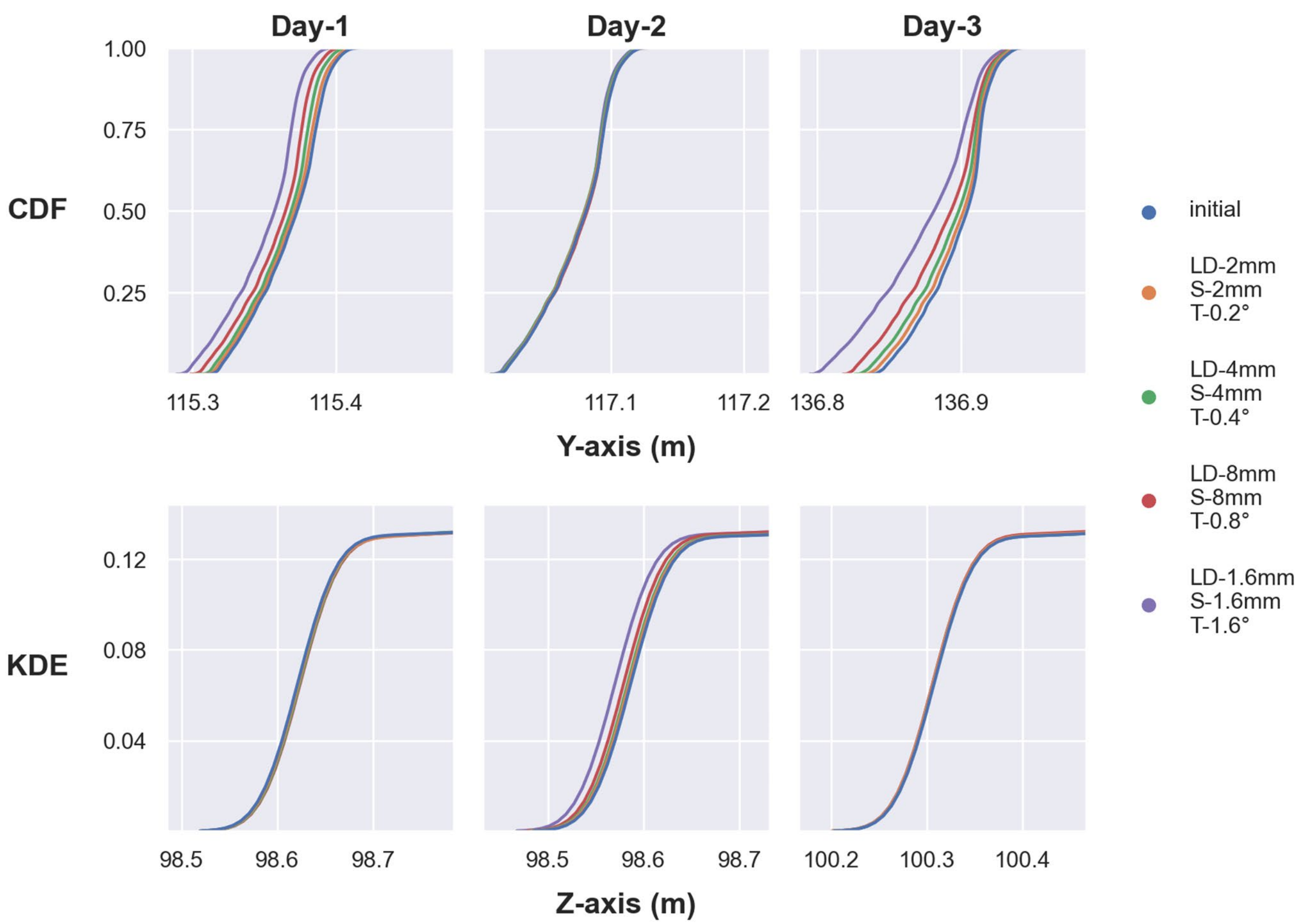

Fig. 9 CDF and KDE plots for the point clouds along the *y*–axis (i.e., the lateral axis) and *z*–axis (i.e., the longitudinal axis along the height of the wooden sheet) for the scans on the three days of experiments (KDE plots show a window of 0.4 m width). The *y*–axis is the lateral axis with respect to the surface of the wooden sheet while the *z*–axis is the longitudinal axis along the height of the wooden sheet. The numbers in the figure represent the location of the point clouds with respect to the origin of the coordinate system as explained in Fig. 2

TLS but can be used to detect potential biases in the deformation estimation.

- Potential differences of the point clouds density between the scans of different epochs can affect the estimated deformation, especially for the deformation of settlement where the deformation is in the point cloud plane and can significantly affect the estimated deformation.
- The use of statistical tools, such as the CDF and KDE functions, can reveal the type of global deformation (i.e., throughout lateral displacement, subsidence and/or tilt about the transverse axis).
- The application of multiple methods to estimate the deformation of the point clouds (i.e., cloud-mean, C2C, C2M, and M3C2 methods) enhances the reliability of the estimated deformation by mitigating the impact of potential biases.
- The parameters settings (e.g., normal scale, projection scale of M3C2 method) for each of the distance calculation methods needs to be appropriately configured so no bias will be introduced in the estimated deformation.

One of the primary limitations of this research is the error caused by the registration of the point clouds. The registration in this research was done using the static points and using a local coordinate system, whereas the registration in real monitoring projects can be done using the global coordinate system using Global Navigation Satellite System (GNSS) measurements, which their uncertainty accumulates to the error of the deformation estimation. Alternatively, the registration can be executed using a local coordinate system but the reference points that are used for the registration process could be moved, which results in a wrong deformation estimation. Another limitation of this research is the use of only three static points, while the increase in number of the reference points can increase the registration accuracy and consequently the accuracy of the deformation estimation. In addition, all the deformation amplitudes (i.e., epochs) were simulated on one day, resulting in the same environmental conditions. These environmental conditions may vary between the epochs in real monitoring projects, which can affect the performance of the TLS.

Future research should mainly focus on testing the optimum point-cloud resolution to optimize the data size as it is one of the main limitations of using the TLS for monitoring retaining structures. Additionally, methods for subsampling the point clouds while keeping the same level of accuracy in detecting the geometric deformations are of great research interest.

Acknowledgements All the gratitude goes to King Saud University and the Saudi Arabian Cultural Bureau in London for their generous sponsorship for the first author Ali Algadhi to complete his PhD studies.

Data availability The raw data supporting the conclusions of this article will be made available by the authors on request.

Declarations

Conflict of interest The authors declare that they have no known competing financial interests or personal relationships that could have appeared to influence the work reported in this paper. The authors declare the following financial interests/personal relationships which may be considered as potential Conflict of interest.

References

1. Acikgoz S, Soga K, Woodhams J (2017) Evaluation of the response of a vaulted masonry structure to differential settlements using point cloud data and limit analyses. Constr Build Mater 150:916–931
2. Al-Rawabdeh A, Aldosari M, Bullock D, Habib A (2020) Mobile LiDAR for scalable monitoring of mechanically stabilized earth walls with smooth panels. Appl Sci 10(13):4480
3. Aldosari M, Al-Rawabdeh A, Bullock D, Habib A (2020) A Mobile LiDAR for Monitoring Mechanically Stabilized Earth Walls with Textured Precast Concrete Panels. Remote Sensing 12(2):306
4. Algadhi A, Psimoulis P, Grizi A, Neves L (2023) Assessment of accuracy and performance of terrestrial laser scanner in monitoring of retaining walls. In 5th Joint International Symposium on Deformation Monitoring
5. Aliberti L, Iglesias Picazo P (2019) Close-Range Photogrammetry Practice: Graphic Documentation of the Interior of the Walls of Avila (Spain). The International Archives of the Photogrammetry, Remote Sensing and Spatial Information Sciences, XLII-2/W15:49–53
6. Athanasopoulos-Zekkos A, Lynch JP, Zekkos D, Grizi A, Admassu KA, Benhamida B, Spino RJ, Mikolajczyk M (2020) Asset Management for Retaining Walls. Available from: http://rgdoi.net/10.13140/RG.2.2.11760.89608 [Accessed 10/05/2024]
7. Besl P, McKay ND (1992) A method for registration of 3-D shapes. IEEE Trans Pattern Anal Mach Intell 14(2):239–256
8. Bolkas D, Martinez A (2018) Effect of target color and scanning geometry on terrestrial LiDAR point-cloud noise and plane fitting. J Appl Geod 12(1):109–127
9. CloudCompare (2021) CloudCompare v2.12 beta [windows 64-bit]. Available from: http://www.cloudcompare.org/ [Accessed 31/12/2023]
10. Jatmiko J, Psimoulis P (2017) Deformation monitoring of a steel structure using 3d terrestrial laser scanner (tls). In Proceedings of the 24th International Workshop on Intelligent Computing in Engineering, pages 10–12, Nottingham, UK. ICE Publishing
11. Jia D, Zhang W, Liu Y (2021) Systematic approach for tunnel deformation monitoring with terrestrial laser scanning. Remote Sens 13(17):3519
12. Kaartinen E, Dunphy K, Sadhu A (2022) LiDAR-Based Structural Health Monitoring: Applications in Civil Infrastructure Systems. Sensors, 22(12)
13. Kalenjuk S, Lienhart W, Rebhan MJ (2021) Processing of mobile laser scanning data for large-scale deformation monitoring of anchored retaining structures along highways. Comput Aided Civil Infrastruct Eng 36(6):678–694. https://doi.org/10.1111/mice.12656
14. Kim M-K, Wang Q, Li H (2019) Non-contact sensing based geometric quality assessment of buildings and civil structures: A review. Autom Constr 100:163–179
15. Kwiatkowski J, Anigacz W, Beben D (2020) A case study on the noncontact inventory of the oldest european cast-iron bridge using terrestrial laser scanning and photogrammetric techniques. Remote Sens 12(17):2745
16. Lague D, Brodu N, Leroux J (2013) Accurate 3d comparison of complex topography with terrestrial laser scanner: Application to the rangitikei canyon (n-z). ISPRS J Photogramm Remote Sens 82:10–26
17. Leica-Geosystems (2018) Leica RTC360 user manual. Available from: https://g2survey.com/user-manuals/ [Accessed 10/05/2024]
18. Li J, Wang L, Huang J (2023) Wall length-based deformation monitoring method of brick-concrete buildings in mining area using terrestrial laser scanning. J Civil Struct Health Monitor 13(4):1077–1090
19. Lienhart W (2017) Geotechnical monitoring using total stations and laser scanners: critical aspects and solutions. J Civil Struct Health Monitor 7:315–324
20. Oats R, Escobar-Wolf R, Oommen T (2017) A novel application of photogrammetry for retaining wall assessment. Infrastructures, 2(3)
21. Oskouie P, Becerik-Gerber B, Soibelman L (2016) Automated measurement of highway retaining wall displacements using terrestrial laser scanners. Autom Constr 65:86–101
22. Ponzo FC, Auletta G, Ielpo P, Ditommaso R (2024) Dinsar-sbas satellite monitoring of infrastructures: how temperature affects the "ponte della musica'' case study. J Civil Struct Health Monitor 14(3):745–761
23. Ponzo FC, Iacovino C, Ditommaso R, Bonano M, Lanari R, Soldovieri F, Cuomo V, Bozzano F, Ciampi P, Rompato M (2021) Transport infrastructure shm using integrated sar data and on-site vibrational acquisitions: "ponte della musica-armando trovajoli" case study. Applied Sciences, 11(14)

24. Rashidi M, Mohammadi M, Kivi S, Abdolvand M, Truong-Hong L, Samali B (2020) A decade of modern bridge monitoring using terrestrial laser scanning: Review and future directions. Remote Sensing 12(22):1–34
25. Ruffhead AC (2021) Derivation of rigorously-conformal 7-parameter 3D geodetic datum transformations. Surv Rev 53(376):8–15
26. Seo H (2021) Tilt mapping for zigzag-shaped concrete panel in retaining structure using terrestrial laser scanning. J Civil Struct Health Monitor 11(4):851–865
27. Seo H, Zhao Y, Chen C (2021) Displacement Estimation Error in Laser Scanning Monitoring of Retaining Structures Considering Roughness. Sensors 21(21):7370
28. Seo H, Zhao Y, Wang J (2019) Monitoring of Retaining Structures on an Open Excavation Site with 3D Laser Scanning. In International Conference on Smart Infrastructure and Construction 2019 (ICSIC), pages 665–672, Cambridge, UK. ICE Publishing
29. Zhao Y, Seo H, Chen C (2022) Displacement analysis of point cloud removed ground collapse effect in smw by canupo machine learning algorithm. J Civil Struct Health Monitor 12(2):447–463